Technical Report Documentation Page

1. Report No.	2. Government Accession No.	3. Recipient's Catalog No.
j.atmosenv.2023.120106		

4. Title and Subtitle	5. Report Date
Accounting for plume rise of aircraft emissions in AERMOD	September 2023
	6. Performing Organization Code

7. Author(s)	8. Performing Organization Report No.
Gavendra Pandey, Akula Venkatram, Saravanan Arunachalam	

9. Performing Organization Name and Address	10. Work Unit No. (TRAIS)
Center of Excellence for: Alternative Jet Fuels and Environment The University of North Carolina at Chapel Hill, USA	11. Contract or Grant No. 13-C-AJFE-UNC-014, 016

12. Sponsoring Agency Name and Address	13. Type of Report and Period Covered
Federal Aviation Administration Office of Environment and Energy	Journal Article
	14. Sponsoring Agency Code

15. Supplementary Notes

16. Abstract

The U.S. Federal Aviation Administration (FAA) uses the Aviation Environmental Design Tool (AEDT) to assess the impact of airport emissions on air quality in and around an airport. AEDT incorporates EPA's (Environmental Protection Agency) regulatory model, AERMOD. The area/volume source algorithm in AERMOD is currently used to treat most airport sources including aircraft, which contribute a major fraction of total airport emissions. Aircraft emissions have horizontal momentum corresponding to the forward thrust of the aircraft. In addition, they have buoyancy corresponding to the heat rejected from the aircraft engine. These plume dynamics are not included in the latest version (v22112) of the area/volume source algorithm in AERMOD; the effects of the plume on ground-level concentrations are accounted through an initial plume height and width based on LIDAR observations at the end of runways. Model predictions based on this approach are likely to lead to overestimates of ground-level concentrations because they do not account for the increase of plume height with distance from the source. This paper proposes a plume rise formulation for aircraft emissions modeled with AERMOD. Plume rise is modeled using the weighted average of the characteristics of the aircraft that pass through the area/volume source during 1 h, the averaging time used in AERMOD. The buoyancy parameter used to compute plume rise is estimated using the aircraft engine characteristics: thrust, fuel burn rate, the velocity of the aircraft, air-fuel ratio, and the engine bypass ratio. The proposed plume rise formulation for AERMOD is evaluated using SO2 observations from the 2012 Air Quality Source Apportionment Study (AQSAS) conducted at the Los Angeles International Airport (LAX). The results from the evaluation indicate that plume rise improves AERMOD's description of the qualitative behavior of concentrations measured in and around the airport.

17. Key Words	18. Distribution Statement
AERMOD, Aircraft, Air quality, Buoyancy, Jet-exhaust, Plume rise, ASCENT	

19. Security Classif. (of this report)	20. Security Classif. (of this page)	21. No. of Pages	22. Price
Unclassified	Unclassified		

Atmospheric Environment 314 (2023) 120106

Contents lists available at ScienceDirect

Atmospheric Environment

journal homepage: www.elsevier.com/locate/atmosenv

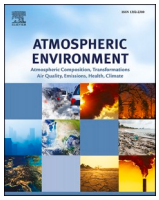

Accounting for plume rise of aircraft emissions in AERMOD

Gavendra Pandey [a], Akula Venkatram [b], Saravanan Arunachalam [a,*]

[a] Institute for the Environment, The University of North Carolina at Chapel Hill, USA
[b] University of California at Riverside, USA

HIGHLIGHTS

- AERMOD doesn't account for aircraft plume dynamics in area/volume source treatment.
- A proposed plume rise formulation for aircraft emissions modeled with AERMOD.
- Account for momentum and buoyancy of jet exhausts that govern aircraft plume rise.
- AERMOD's concentrations with plume rise are relatively insensitive to wind speed.
- Results demonstrate improved model performance after incorporating plume rise.

ARTICLE INFO

Keywords:
AERMOD
Aircraft
Air quality
Buoyancy
Jet-exhaust
Plume rise

ABSTRACT

The U.S. Federal Aviation Administration (FAA) uses the Aviation Environmental Design Tool (AEDT) to assess the impact of airport emissions on air quality in and around an airport. AEDT incorporates EPA's (Environmental Protection Agency) regulatory model, AERMOD. The area/volume source algorithm in AERMOD is currently used to treat most airport sources including aircraft, which contribute a major fraction of total airport emissions. Aircraft emissions have horizontal momentum corresponding to the forward thrust of the aircraft. In addition, they have buoyancy corresponding to the heat rejected from the aircraft engine. These plume dynamics are not included in the latest version (v22112) of the area/volume source algorithm in AERMOD; the effects of the plume on ground-level concentrations are accounted through an initial plume height and width based on LIDAR observations at the end of runways. Model predictions based on this approach are likely to lead to overestimates of ground-level concentrations because they do not account for the increase of plume height with distance from the source. This paper proposes a plume rise formulation for aircraft emissions modeled with AERMOD. Plume rise is modeled using the weighted average of the characteristics of the aircraft that pass through the area/volume source during 1 h, the averaging time used in AERMOD. The buoyancy parameter used to compute plume rise is estimated using the aircraft engine characteristics: thrust, fuel burn rate, the velocity of the aircraft, air-fuel ratio, and the engine bypass ratio. The proposed plume rise formulation for AERMOD is evaluated using SO_2 observations from the 2012 Air Quality Source Apportionment Study (AQSAS) conducted at the Los Angeles International Airport (LAX). The results from the evaluation indicate that plume rise improves AERMOD's description of the qualitative behavior of concentrations measured in and around the airport.

1. Introduction

Airports are essentially mini-cities that accommodate all the facilities and activities required to serve the thousands of people who pass through the airport each day. The aircraft that transport passengers in and out of an airport account for a significant fraction of the pollutant emissions from an airport. Their impact on air quality within and outside the airport requires attention to their unique characteristics. A large fraction of the aircraft emissions during the total flight cycle from gate to gate originate from aircraft engines specifically during landing and takeoff operations (LTO). Unlike emissions from stationary sources, aircraft emissions are transient, lasting for a few minutes to a fraction of an hour depending on how busy the airport is. The emissions, which originate from moving sources, have horizontal momentum corresponding to the forward thrust of the aircraft. In addition, they have buoyancy corresponding to the heat rejected from the aircraft engine. A

* Corresponding author. Institute for the Environment, The University of North Carolina at Chapel Hill, Chapel Hill, NC, 27517, USA.
E-mail address: sarav@email.unc.edu (S. Arunachalam).

https://doi.org/10.1016/j.atmosenv.2023.120106
Received 10 February 2023; Received in revised form 14 September 2023; Accepted 18 September 2023
Available online 19 September 2023

realistic model for the dispersion of these emissions must account for these unique source characteristics.

A handful of studies have examined the impact of airports on surrounding air quality. In almost all of them, models designed for stationary sources have been adapted for aircraft sources. For example, the U.S. Federal Aviation Authority (FAA) incorporates EPA's (Environmental Protection Agency) regulatory model AERMOD (Cimorelli et al., 2005) in their Aviation Environmental Design Tool (AEDT) ("FAA: Aviation Environmental Design Tool (AEDT)," 2014). Aircraft moving in an area of the airport is modeled in the aggregate as an area or volume source. The special features of aircraft sources are accounted through an initial plume height and width based on LIDAR observations made by Wayson et al. (2008). The momentum and buoyancy of jet exhausts that govern plume rise are not incorporated explicitly in computing ground-level concentrations, which might lead to overestimates, as shown in previous studies (Arunachalam et al., 2017).

LASPORT (Janicke and Janicke, 2007), a model used in several countries in Europe, estimates the impact of airport sources by following the motion of Lagrangian particles emitted from the sources. Available descriptions of the model indicate that the horizontal momentum of jet exhausts is included in the initial velocity of the emitted particles, but the effects of plume buoyancy are not treated explicitly in the model.

ADMS-Airport, used primarily in the United Kingdom (UK), does incorporate a detailed treatment of plume rise (Carruthers et al., 2011; CERC, 2020), which presumably accounts for momentum as well as buoyancy of jet exhausts. The description suggests that the model for plume rise also treats the effects of acceleration and deceleration of aircraft on runways on plume rise. However, because the model is proprietary, and the available description of the plume rise model does not contain enough detail to assess its efficacy or evaluate its performance against observations.

The objective of this paper is to suggest an approach to the modeling of plume rise of aircraft emissions that can be incorporated into AERMOD. This will extend the applicability of AERMOD to estimating the impact of airport emissions on air quality at receptors of regulatory interest. Before describing the approach to modeling of plume rise, we provide observational evidence of the potential importance of modeling plume rise of aircraft emissions.

1.1. Observations of plume rise

Measurements of the initial behavior of aircraft plumes are limited. A LIDAR study of aircraft plume rise and spread at Los Angeles International Airport (LAX) by Wayson et al. (2004) and at Hartsfield-Jackson Atlanta International Airport (ATL) and Denver International Airport by Wayson et al. (2008) indicated that the plumes from aircraft exhausts were elevated by tens of meters. But these measurements are confined to the length of the runway when the plume is essentially horizontal and is in contact with the ground, and the vertical growth of the plume is governed by the shear between the velocity of the gases in the plume and the ambient velocity. As far as we are aware, there are no direct measurements of the behavior of the aircraft plume when buoyancy becomes the major force in the vertical rise and dispersion of the exhaust plume.

Carslaw et al. (2008, 2006) provide indirect evidence on the role of buoyancy on plume behavior through their analysis of NO_x concentrations measured near two runways at Heathrow airport in London. The airport has two runways that lie roughly along the east-west axis so that aircraft can take advantage of the prevailing westerly winds. Carslaw et al. (2006) show that hourly averaged concentrations of NO_x at a location 180 m north of the northern runway varied little with wind speed (Fig. 1). This indicates the significant role of buoyancy of the jet plume in governing ground-level concentrations. The concentration, C, associated with a near ground-level source with no buoyancy would be sensitive to wind speed because $C \sim 1/U$, where U is the wind speed. On the other hand, a buoyant source would be relatively insensitive to the wind speed because the decrease in dilution with wind speed is compensated by the decrease in buoyant plume rise with wind speed. This is an indication, though indirect, that the inclusion of plume rise is likely to improve the performance of models for dispersion of aircraft emissions. The next section describes our proposed approach on plume rise formulation for aircraft exhausts.

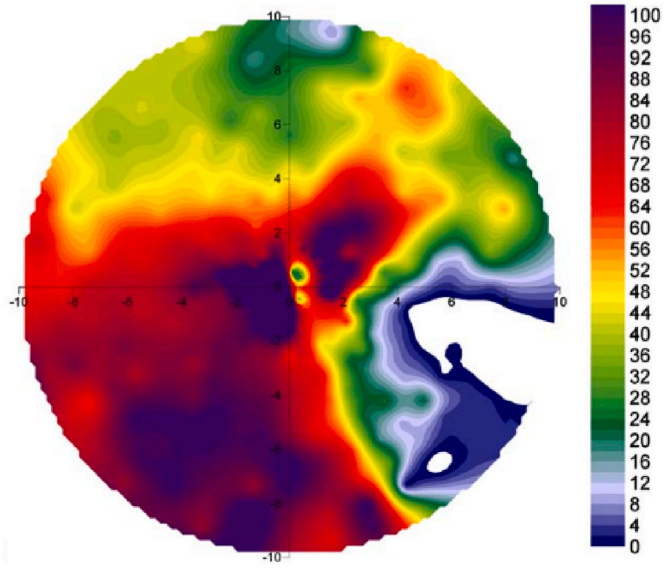

Fig. 1. Bivariate polar plot of wind speed and NO_x concentrations ($\mu g/m^3$) as a function of wind direction (Source: Carslaw et al. (2006)).

Emissions from the north runway in Heathrow originate from the south, southwest direction. Note that the highest concentrations vary little with wind speed.

2. Aircraft engines

Before describing the details of the proposed plume rise formulation, we first review the different types of aircraft engines and their characteristics that are relevant to plume rise. Aircraft engines can be grouped into two categories. The first category is turbine-based: turbojet and turbofan engines. The exhaust from these engines has both buoyancy and horizontal momentum. The second category includes shaft-based engines: turboprop, turboshaft, and piston engines, in which the exhaust might not possess horizontal momentum. A detailed description of each type of engine is given in the supplementary material/information of this paper.

2.1. Turbine-based engines

Fig. 2 shows the operation of a modern turbofan engine.

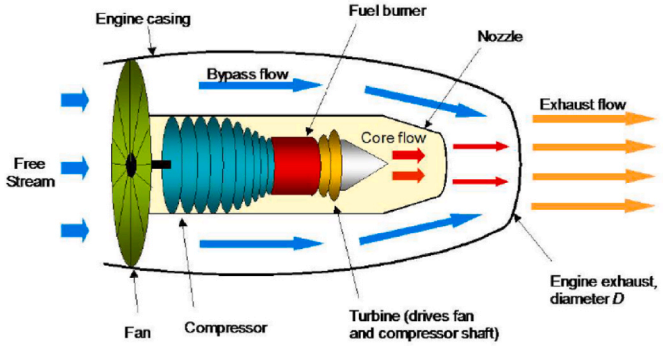

Fig. 2. Schematic of turbofan jet engine. (Source: ADMS-Airport Manual (CERC, 2020)).

In an aircraft powered with a turbine-based engine, air enters the engine at roughly the speed of the aircraft relative to the moving aircraft. A fraction of the incoming air is directed into the core, where it is first compressed, then enters the combustion where the injected fuel increases the energy of the gases, which then drives a gas turbine. The gas turbine generates enough power to drive the compressor and the fan. The core flow is then exhausted through a nozzle. A turbojet engine lacks a fan, and all the air passes through the core.

In a modern turbofan engine, most of the air entering the engine "bypasses" the core as it is driven towards the exit by the fan at the entrance. The mass flow rate of the bypass air is several times that of the core air; the ratio of the two mass flow rates is known as the bypass ratio, which is denoted by *bypr*. The bypass ratio of modern turbofan engines is greater than 5. The exiting air is a mixture of core air and bypass air, and the average velocity of the two streams is much smaller than that of the core air. Low bypass turbofans are commonly used in fighter jet engines and have ratios in the 0.30 to 0.50 range, while modern high bypass engines may have a ratio as high as 9 or 10 (Herbert, 2022).

The thrust of the engine is the product of the total mass flow rate and the difference between the inlet and exit velocities. As we will see, the power associated with propulsion is maximized by bringing the exit velocity of the exhaust gases as close as possible to the inlet velocity, and at the same time increasing the mass flow rate through the engine. This is achieved through as large a bypass ratio as possible, which involves making the fan as large as possible.

The ratio of the mass of air entering the core to that of the fuel injected into the combustion chamber is known as the air-fuel ratio, denoted here by *AF*. Although the stoichiometric *AF* ratio is about 15, it is maintained at values greater than 45 to ensure that the temperature of the gases exiting the combustion chamber is below that required for the integrity of the turbine blades. The ratio of the mass flow rate of air plus fuel, $\dot{m}$, to that of the fuel, $\dot{m}_f$, is approximately $AF(1 + bypr)$, which is over 200 for most aircraft engines. Therefore, the mass flow rate through the engine is essentially that of air. We now have the necessary background to relate the buoyancy parameter to the characteristics of an aircraft engine.

3. Proposed approach

In principle, we can compute the impact of aircraft emissions by following the motion of each aircraft in an airport. Because this approach is not compatible with AERMOD's framework, which assumes that the emissions are stationary. We represent the moving aircraft as sources contributing to emissions from an area source. The total emission over the specified area is the sum of the emissions that occur while the aircraft travel over the area. Consider a specific area A in the airport. During a time period, typically an hour, assume that N aircraft pass through this area each of which emits e_i of a pollutant during its passage through the area. Then the emission rate from the area is

$$E = \frac{\sum_{i=1}^{N} \dot{e}_i \Delta t_i}{AT} \tag{1}$$

where Δt_i is the time spent by the i^{th} aircraft in A while emitting at a rate $\dot{e}_i$, and $T = 3600\ s$. This then allows us to treat emissions from moving aircraft as a stationary source, specifically from a fixed area source.

The plume rise of emissions from each area source is computed with the relevant characteristics of a typical aircraft that passes through the area A, which is described with a convex polygon, as in AERMOD. The engine parameters are computed as normalized characteristics for each fixed source by taking the average of all the flight segment values within an area source during each hour, weighted by the fuel burn contribution of each segment. Equation (2) shows how the Aviation Environmental Design Tool (AEDT) weights each of these characteristics,

$$\dot{m}_{f_k} = \frac{\sum_{a=a_{1,k}}^{A_k} \sum_{t=t_{1,k}}^{T_k} w_{k,a,t} Fb_{a,t} m_{a,t}}{\sum_{a=a_{1,k}}^{A_k} \sum_{t=t_{1,k}}^{T_k} w_{k,a,t} Fb_{a,t}}, \tag{2}$$

where $\dot{m}_{f_k}$ is a normalized plume rise characteristic, for example, fuel burn rate, for a cuboid k; $Fb_{a,t}$ is a total fuel burn of the flight trajectory segment t of the air operation a; $m_{a,t}$ is the true fuel burn rate of the flight trajectory segment t of the air operation a; $w_{k,a,t}$ is the weight of the subsegment of the flight trajectory segment t of the air operation a, which resides in the cuboid k; the air operation and trajectory segment ranges, $\{a_{1,k}, A_k\}$ and $\{t_{1,k}, T_k\}$, respectively, could vary from one cuboid to another. The $w_{k,a,t}$ is expressed as follows:

$$w_{k,a,t} = \frac{\tau_{k,a,t}}{\tau_{a,t}} \tag{3}$$

where $\tau_{k,a,t}$ is the time trajectory segment t of the air operation a spends in the cuboid k, and $\tau_{a,t}$ is the total duration of the segment t of the air operation a.

We compute the other variables, described later, that govern plume rise in a similar manner.

When an aircraft travels in the airport, it lays down a plume along its path (Fig. 3). It is useful to think of a line thermal (Arunachalam et al., 2017) as a cylinder that contains the energy rejected by the engines. If t is the time spent by an aircraft in an area source, the length of the air cylinder affected by emissions of the aircraft traveling at an average speed, v_a, into a head wind, U_{eff} is $(v_a + U_{eff})t$. If Q_e is the heat rejected per unit time by the aircraft, the heat content per unit length of the thermal is $Q_e/(v_a + U_{eff})$. We realize that the ambient U_{eff} is not always opposed to v_a. However, because the area source treatment of emissions does not trace the path of every aircraft in a source area, we add the velocities to ensure that we recover the expression for plume rise when v_a is close to zero or is large compared to U_{eff}.

We incorporate this expression for energy content per unit length of the line thermal into the familiar buoyancy parameter, F_b, used to compute plume rise from a point source: (Briggs, 1965):

$$F_b = \frac{g}{T_a} v_e r_0^2 (T_e - T_a), \tag{4}$$

where v_e *and* T_e are the velocity and temperature of the exhaust plume, T_a is the ambient temperature, g is the acceleration due to gravity, and r_0 is the effective radius of the point source. Equation (4) can be re-written as

$$F_b = \frac{g}{T_a} \frac{Q_e}{\pi \rho_e C_p}, \tag{5}$$

where Q_e is the heat rejected by the aircraft engine, ρ_e, is the density and C_p is the specific heat of the exhaust gases.

Once an aircraft creates a line thermal in its path in an area source, the line thermal becomes detached from the aircraft and its behavior is governed by the energy and momentum that it contains. The buoyancy associated with unit length of the line thermal is $F_b/(v_a + U_{eff})$, and the plume rise, h_{pb}, of the elements of the line thermal associated with a representative aircraft in the area source is (Venkatram and Schulte, 2018):

$$h_{pb} = \left(\left(\frac{r_0}{\beta} \right)^3 + \frac{3}{2\beta^2} \frac{F_b}{(v_a + U_{eff})} \left(\frac{x}{U_{eff}} \right)^2 \right)^{1/3} - \left(\frac{r_0}{\beta} \right), \tag{6}$$

where $\beta = 0.6$ is an entrainment constant, x is the effective distance between the source and receptor, and U_{eff} is the effective velocity that governs transport of the elements of the line thermal, and r_0 is the initial radius of the line thermal. The travel time from source to receptor is

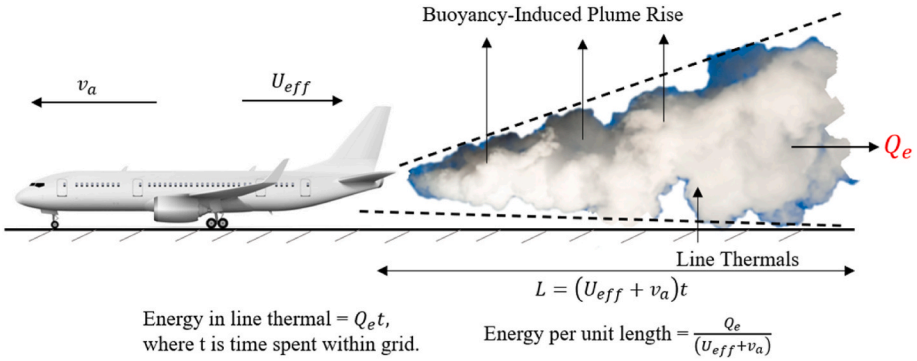

Fig. 3. Schematic of a line thermal behind an airplane at surface.

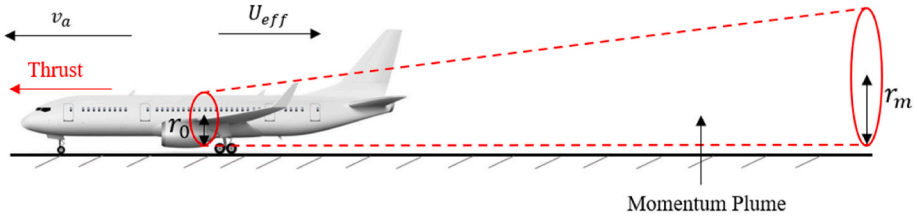

Fig. 4. Schematic of a momentum plume rise due to the aircraft's forward thrust.

x/U_{eff}, where the effective distance, x, is measured from the center of mass of the area source. Note that Equation (6) reduces to the plume rise equation for stationary sources if the speed of the aircraft, v_a, is zero.

In addition to buoyancy, plume rise is also governed by horizontal momentum of the exhaust gases, which in turn depends on the thrust generated by an engine.

3.1. Accounting for jet momentum

We assume that the horizontal momentum is conserved as the radius of the horizontal plume grows with distance from an aircraft within the area source (Fig. 4).

For a top-hat profile of velocity within the plume, the momentum balance can be written as

$$\rho_p U_p (U_p - U_a)\pi r^2 = T, \tag{7}$$

where ρ_p is the plume density. U_p is the velocity inside the plume U_a is the ambient velocity at the level of the plume, where these velocities are measured relative to the moving aircraft, so that $U_a = v_a + U_{eff}$. The initial momentum flow inside the plume is the thrust, T, exerted by the engine on the air. A version of this equation is derived in the Appendix A1 of Arunachalam et al. (2017).

As in Barrett et al. (2013), we assume that the radius of the jet exhaust grows linearly with distance from a point within the area source

$$r = \alpha x + r_0, \tag{8}$$

where $\alpha = 0.1$ is an entrainment constant, and r_0 is the radius of the engine exhaust. This estimate of the radius of the plume allows us to calculate the velocity of air, U_p, inside the plume from Equation (7)

$$U_p = (v_a + U_{eff})\left[0.5 + 0.5\left(1 + \frac{4T}{\pi r^2 \rho_p (U_{eff} + v_a)^2}\right)^{1/2}\right], \tag{9}$$

The radius of the momentum plume is taken to grow until the difference between the plume and ambient velocities is comparable to the standard deviation of the ambient horizontal velocity fluctuations, $\sigma_u = 2.0u_*$, where u_* is the surface friction velocity. Then, the maximum plume radius is given by the relationship

$$T = \pi \rho_a r_m^2 \left((v_a + U_{eff}) + \sigma_u\right)\sigma_u, \tag{10}$$

where ρ_a is the ambient density. Then r_m is given by

$$r_m = \left(\frac{T}{\pi \rho_a \left((v_a + U_{eff}) + \sigma_u\right)\sigma_u}\right)^{1/2}. \tag{11}$$

The plume rise associated with momentum, h_{pm}, is taken to be the radius of the plume

$$h_{pm} = \begin{cases} r_o + \alpha x, & x \le x_m \\ r_m, & x > x_m \end{cases}, \tag{12}$$

where x_m is the distance at which the radius reaches its maximum value

$$x_m = \frac{(r_m - r_0)}{\alpha}. \tag{13}$$

The effect of buoyancy is treated by assuming that it acts independently on the expanding jet plume. However, buoyancy is allowed to interact with horizontal momentum through the initial radius, R_0, which is taken to be the average value of the radius of the momentum plume between 0 and x,

$$R_0 = \frac{1}{x}\int_0^x r(x)dx, \tag{14}$$

which yields

$$R_0 = \begin{cases} r_0 + \alpha x/2, & x \le x_m \\ \frac{x_m}{x}\left(r_0 + \frac{\alpha x_m}{2}\right) + r_m\left(1 - \frac{x_m}{2}\right), & x > x_m \end{cases}, \tag{15}$$

Equation (15) must be solved iteratively because the wind speed at plume height is not known a priori.

The total plume rise is then

$$h_p = h_{pb} + h_{pm}, \tag{16}$$

where the second term on the right-hand side is the plume rise associated with the momentum, which is negligible for turboshaft or piston

engines.

3.2. Maximum plume rise calculation

The rise of the plume associated with buoyancy is limited to the height at which the standard deviation of the vertical velocity fluctuations, σ_w, is equal to the rate of rise of the plume $dh_{pb}/\ dt$. The travel time, t_{max}, associated with maximum plume rise is then given by the solution of the non-linear algebraic equation (Venkatram and Schulte, 2018):

$$\frac{dh_{pb}}{dt} = \frac{d}{dt}\left[\left(\left(\frac{R_0}{\beta}\right)^3 + \frac{3}{2\beta^2}\frac{F_b}{(v_a + U_{eff})}t^2\right)^{1/3} - \frac{R_0}{\beta}\right] = \sigma_w$$

or

$$\left(\left(\frac{R_0}{\beta}\right)^3 + \frac{3}{2\beta^2}\frac{F_b}{(v_a + U_{eff})}t^2\right)^{-\frac{2}{3}}\left(F_b/(v_a + U_{eff})\right)t = \sigma_w\beta^2, \tag{17}$$

Equation (17) is solved using Bi-section to yield t_{max}. Note that the solution of Equation (17) accounts for the plume spread induced by momentum, R_0. The maximum plume rise is then given by Equation (6) in which $t = t_{max}$.

When the boundary layer is stable, plume rise is limited by the final rise in a stable atmosphere with a potential temperature gradient

$$h_{max} = 2.66\left(\frac{F_b}{(v_a + U_{eff})N^2}\right)^{1/3}, \tag{18}$$

where N is the Brunt-Vaisala frequency,

$$N = \left(\frac{g}{T_a}\frac{d\theta}{dz}\right)^{1/2} \tag{19}$$

The total plume rise is also limited by the height of the mixed layer.

3.3. Treatment of airborne sources

Airborne emissions are assumed to originate from fixed-point sources along the path of an aircraft. The emissions along the landing or takeoff path are assigned to the point sources between two levels in a manner similar to that used to assign surface emissions to area sources. We assume that the momentum jet is directed along the flight path until it runs out of momentum. This distance along the flight path at which buoyancy takes over is x_m given by Equation (13). If θ is the angle with the horizontal at which the aircraft is landing or taking off, we assume that the plume descends by $h_p = x_h\ tan\ \theta$ in the range of horizontal distance $x_h <= x_m\ cos\ \theta$. Buoyancy governs plume rise beyond $x_h = x_m\ cos\ \theta$, so that plume rise beyond this distance becomes

$$h_p = z_s - x_m\ sin\ \theta + h_{pb}, \tag{20}$$

where z_s is the airborne source height, and h_{pb} is the buoyant plume rise given by the equations described previously. The next sections describe the calculation of plume rise parameters using aircraft engine characteristics.

3.4. Computing buoyancy parameter from engine characteristics

3.4.1. Turbine-based engines

The exhaust temperature and rejected heat required in Equation (5) to compute the buoyancy parameter are not available for jet/gas turbine engines. Thus, it is necessary to estimate these variables using the available engine characteristics: the thrust, T, the aircraft velocity, v_a, fuel burn rate, $\dot{m}_f$, the air-fuel ratio, AF, and the bypass ratio, $bypr$.

We can derive an expression for Q_e by writing the energy balance

$$\dot{m}_f H_f \eta_c = \frac{\dot{m}}{2}\left(v_e^2 - v_a^2\right) + Q_e, \tag{21}$$

where $\dot{m}_f$ is the fuel consumption rate, and H_f is the heating value of the fuel. The combustion efficiency, η_c, is close to unity. The air mass flow rate, $\dot{m}$, is related to the fuel burn rate, $\dot{m}_f$, through

$$\dot{m} = \dot{m}_f AF(1 + bypr), \tag{22}$$

where AF is the air-fuel ratio, and $bypr$ is the engine bypass ratio.

Equation (21) states that the power supplied by the fuel (left-hand side) is the sum of the increase in kinetic power and thermal power added to the air passing through the engine.

The average exhaust velocity, v_e, of the gases from the engine follows from the expression for thrust

$$T = \dot{m}(v_e - v_a), \tag{23}$$

where v_a is the aircraft velocity, so that

$$v_e = v_a + \frac{T}{\dot{m}}. \tag{24}$$

Equations (22) and (24) provide $\dot{m}_f$ and v_e required to compute Q_e, from Equation (21).

Then, the preceding equations allow us to compute the buoyancy parameter, F_b, from

$$F_b = \frac{g}{T_a}\frac{Q_e}{\pi C_p \rho_e}, \tag{25}$$

where the exit density, ρ_e, is computed from the energy conservation equation and the equation of state,

$$\rho_e = \frac{p_a}{R_a T_e}, \tag{26}$$

$$T_e = \frac{Q_e}{\dot{m}C_p} + T_a, \tag{27}$$

where p_a is the ambient pressure, and R_a is the gas constant of air. We see that the inputs required to compute F_b are the thrust, T, the aircraft velocity, v_a, the fuel burn rate, $\dot{m}_f$, the air-fuel ratio, AF, and the engine bypass ratio, $bypr$.

3.4.2. Shaft-based engines

The turboshaft engine is another common type of jet/gas turbine engine. It delivers power to a shaft that drives something other than a propeller. The biggest difference between a turbojet and turboshaft engine is that: in a turboshaft engine, most of the energy produced by the expanding gases is used to drive a turbine rather than produce thrust. Many helicopters use a turboshaft gas turbine engine. In addition, turboshaft engines are widely used as auxiliary power units on large aircraft (Aeronautics-Guide, 2022).

In a turboshaft engine, the propeller is driven by a gas turbine. The air passing through the propeller is not heated. So, the hot exhaust from the turbine constitutes the primary source of buoyancy. The heat ejected by the turbine can be estimated if the compression ratio of the compressor in the turbine, CR, is specified. The compression ratio is the ratio of the stagnation pressures at the outlet and inlet of the compressor.

For an ideal turbine, CR, determines the thermal efficiency of the turbine, which is given by

$$\eta_t = 1 - \frac{1}{\alpha_1} \tag{28}$$

$$\alpha_1 = CR^{\frac{k-1}{k}}, \tag{29}$$

where $k = \frac{C_p}{C_v} = 1.4$ is the ratio of the specific heats of air at constant

pressure and volume.

The alternate way to determine the thermal efficiency of the turbine is as

$$\eta_t = \frac{p_s P_r}{\dot{m}_f H_f}, \tag{30}$$

where p_s is the power setting and P_r is the rated power.

Then, the power transferred to the propeller is $W = \dot{m}_f H_f \eta_t$ and the heat rejected is

$$Q_e = \dot{m}_f H_f (1 - \eta_t) = \frac{\dot{m}_f H_f}{\alpha_1}, \tag{31}$$

where H_f is the heating value of the fuel, and $\dot{m}_f$ is the fuel rate.

The temperature of the exhaust is seen to be

$$T_e = T_a + \frac{(1 - \eta_t) H_f}{C_p AF}, \tag{32}$$

where AF is the air-fuel ratio.

This temperature is used to compute the density assuming that the pressure is ambient, p_a,

$$\rho_e = \frac{p_a}{R_a T_e}. \tag{33}$$

This density is used in the formula for the buoyancy parameter Equation (25).

4. Impact of plume dynamics on ground-level concentrations

We first provide estimates of plume rise associated with aircraft emissions as a function of aircraft speed and ambient velocity. We then estimate of the impact of the plume rise formulation on ground-level concentrations of SO_2 using data from the Los Angeles Source Apportionment Study (LAX AQSAS Phase III).

The final plume rise in an unstable boundary layer is proportional to $F_b/((U_{eff} + v_a)\sigma_w^2)$ and the distance to final rise is proportional to $\left(\frac{F_b}{\sigma_w^3}\right)\left(\frac{U_{eff}}{U_{eff}+v_a}\right)$ if we neglect the initial radius R_0 in Equation (17). These results reflect the impact of the aircraft speed, v_a, in determining plume rise through its role in governing the energy imparted to unit length of the line thermal laid down by the moving aircraft.

Fig. 5 shows that that the magnitudes of total plume rise corresponding to engine characteristics of a typical aircraft, which is operating in LAX during take-off and taxiing. The buoyancy parameter during take-off is 1864 m^4/s^3, reflecting full power, is about 38 times the 49 m^4/s^3 during taxiing. The thrust of 88242 N is about 15 times that during taxiing. These differences in engine parameters are reflected the variations of plume rise with effective wind speed and aircraft speed shown in Figs. 5 and 6. The meteorological variables correspond to daytime when the planetary boundary layer height (PBL) as 960 m, and the standard deviation of the vertical velocity fluctuations, σ_w, is 0.71 m/s.

The top panel of Fig. 5 shows that the final plume rise and the distance to final rise are sensitive to aircraft speed when the effective wind speed is 2 m/s. The final plume rise increases from about 150 m to 350 m when the aircraft speed decreases from 60 m/s to 20 m/s. The final plume rise decreases as the wind speed increases as seen in the middle panel of Fig. 5, and the distance at which the plume reaches its final height increases with wind speed, as expected. This effect is seen clearly in the bottom panel when the wind speed increases to 8 m/s.

Fig. 6 shows similar effects of aircraft speed and effective wind speed on plume rise during taxiing. The smaller buoyancy of 49 m^4/s^3 is reflected in the much smaller buoyancy-induced plume rise of less than 20 m; this is compensated to some extent by a decrease in aircraft speed resulting in net decrease of about a factor of 10 even though the buoyancy decreases by a factor of 30. We see that the momentum-induced plume rise is much more important during taxiing and can exceed that induced by buoyancy as seen in the top panel of Fig. 6. Recall that the maximum momentum-induced plume rise is proportional to $\left(\frac{T}{U_{eff}+v_a}\right)^{1/2}$. So, the decrease in thrust accompanied by an aircraft speed factor from take-off to taxiing translates into a reduction by half in momentum plume rise when the effective wind speed is 2 m/s; compare the top panels of Figs. 5 and 6.

We see that an increase in wind speed and aircraft decreases plume rise at a fixed distance from a stationary point in the area source used to

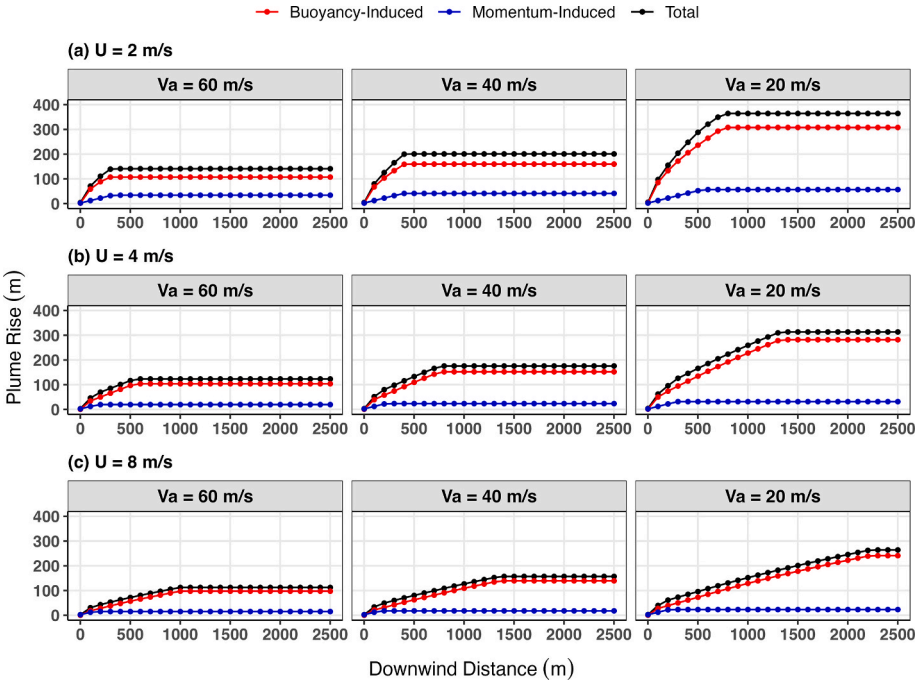

Fig. 5. Variation of momentum and buoyancy induced plume rise with aircraft and ambient velocities for a typical aircraft during take-off. Thrust = 88242 N, Buoyancy parameter = 1863 m^4/s^3.

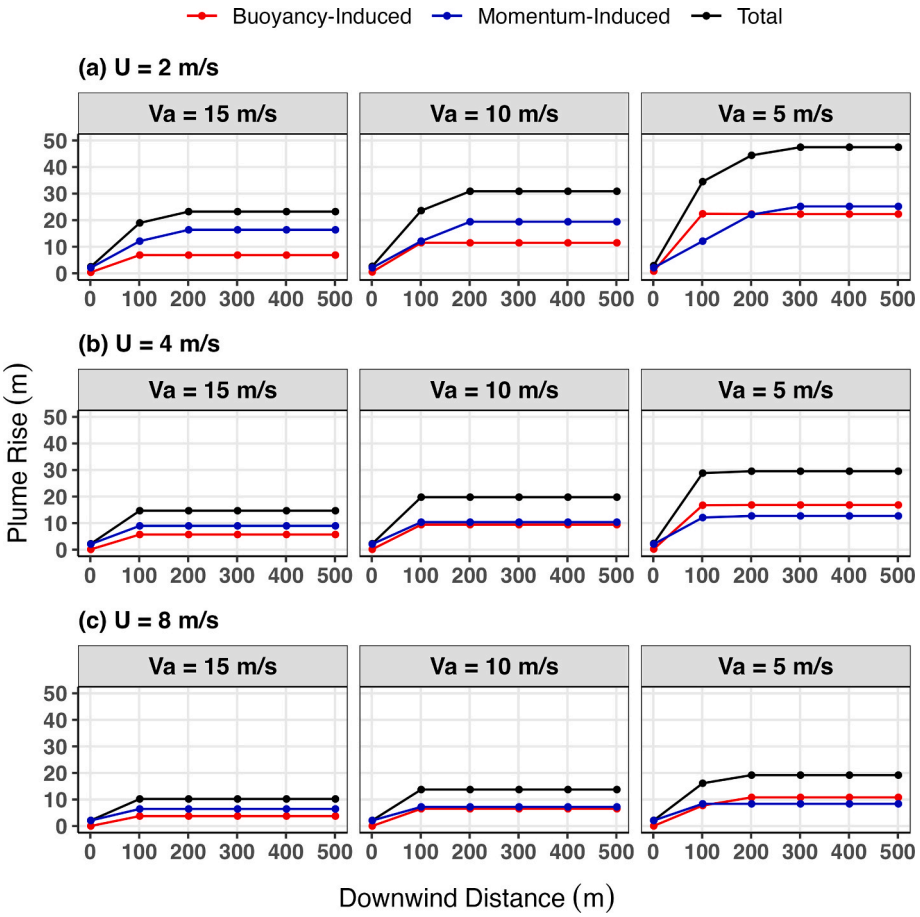

Fig. 6. Variation of momentum and buoyancy induced plume rise with aircraft and ambient velocities for a typical aircraft during taxiing. Thrust = 5741 N, Buoyancy parameter = 49 m^4/s^3.

model emissions from aircraft moving within an area. The concentration at a receptor decreases with the transporting wind speed but increases when the plume rise decreases as the wind speed increases. Thus, the concentration at a receptor should be relatively insensitive to wind speed if these two effects compensate for each other. To see this effect on modeled concentrations, we implement this plume rise approach into AERMOD (v22112). We next search for this behavior by comparing model results with measurements made at Los Angeles airport in 2012.

The Los Angeles Source Apportionment Study was conducted in 2012 in two different monitoring seasons, the "winter measurement season"

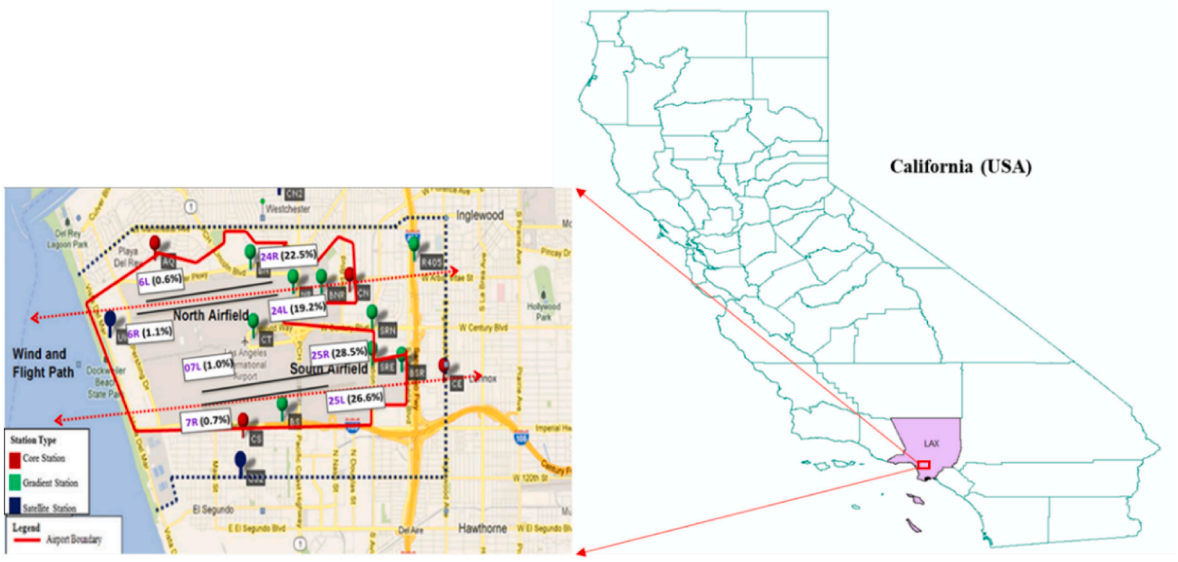

Fig. 7. Locations of core, gradient, and satellite monitoring stations at LAX during AQSAS Phase III (Adapted from (Arunachalam et al., 2017; Pandey et al., 2022), ACRP Report 179).

from 1/31/12 to 3/13/12 and the "summer measurement season" from 7/18/12 to 8/28/12 at the four core sites, the Air Quality (AQ) site, the Community North (CN) site, the Community South (CS) site, and the Community East (CE) site (Fig. 7).

Here, we focus on data at two core sites, CN and CE, which are downwind of the airport. The CN core monitoring site is located at Westchester about 1.5 km east of the North Airfield. The monitoring site CE is located at Lennox about 1.5 km east of the South Airfield and approximately half km east of the I-405 Freeway in Fig. 6 (Tetra Tech, 2013; Arunachalam et al., 2017).

The parameters for turbofan and shaft-based engines required to compute plume rise were generated using the Aviation Environmental Design Tool (AEDT) (FAA, 2014) in the form of AERMOD ready input files (e.g., INP and.HRE files) by Federal Aviation Administration's (FAA) contractor, Volpe Center for Los Angeles airport during both the seasons of 2012.

The meteorological inputs for both seasons of 2012 were generated with AERMET using the KLAX (Los Angeles Airport) surface observations (WBAN 722950), and KNKX (San Diego Marine Corps Air Station) upper air soundings (WBAN 722930).

Fig. 8 shows the average SO_2 hourly concentrations at CN and CE respectively filtered by wind direction in the two seasons. The modeled (with and without plume rise) and observed concentrations only correspond to westerly winds (>180°) to capture the maximum impact of airport sources. Each point in the plot is the average over the concentrations measured during a wind speed interval shown on the *x*-axis.

We see that the measured SO_2 concentration varies by less than 4 $\mu g/m^3$ over a wide range of wind speeds, ranging from 1 to 13 m/s both at CN and CE in the winter, and in the summer period it varies by less than 4 $\mu g/m^3$ over 0 – 8 m/s. Without plume rise, the AERMOD modeled values follow the expected behavior of concentrations associated with surface releases: high concentrations at low wind speeds and concentrations decreasing as the wind speed increases at both CN and CE (Fig. 8). On the other hand, with plume rise, the concentrations are relatively insensitive to wind speed. Although the SO_2 concentrations are underestimated by AERMOD, this insensitivity of modeled concentrations to wind speed is consistent with that observed by (Carslaw et al., 2006) at Heathrow airport. The gap between measured and modeled concentrations is likely associated with emissions from non-aircraft sources in the airport study region that were not modeled in this exercise.

We demonstrate the impact on model performance of implementing the plume rise algorithm in AERMOD v22112 through a quantile-quantile (Q-Q) distribution analysis, which is used by the USEPA for regulatory applications (Perry et al., 2005). Fig. 9 compares the distribution of model-estimated hourly SO_2 concentrations with that of hourly SO_2 concentrations measured at the CN and CE sites during the winter and summer field studies. In this analysis, the modeled concentrations include modeled background sources in addition to aircraft sources, which incorporate plume rise in one of the two distributions shown in Fig. 9. We see that the mid to high modeled concentrations at CN and CE are reduced by including plume rise in AERMOD, and the distribution of modeled concentrations is drawn closer to that of the measured concentrations. This is tentative support for the benefit of incorporating plume rise in modeling the impact of aircraft sources.

5. Conclusions

The objective of this paper is to suggest an approach to the modeling of plume rise of aircraft emissions that can be incorporated into AERMOD. This will extend the applicability of AERMOD to estimating the impact of airport emissions on air quality at receptors of regulatory interest. The proposed approach accounts for plume rise associated with buoyancy and horizontal momentum of exhaust emissions from aircraft engines. The emissions are assumed to originate from line thermals created by an aircraft as they move over the airport. The plume rise

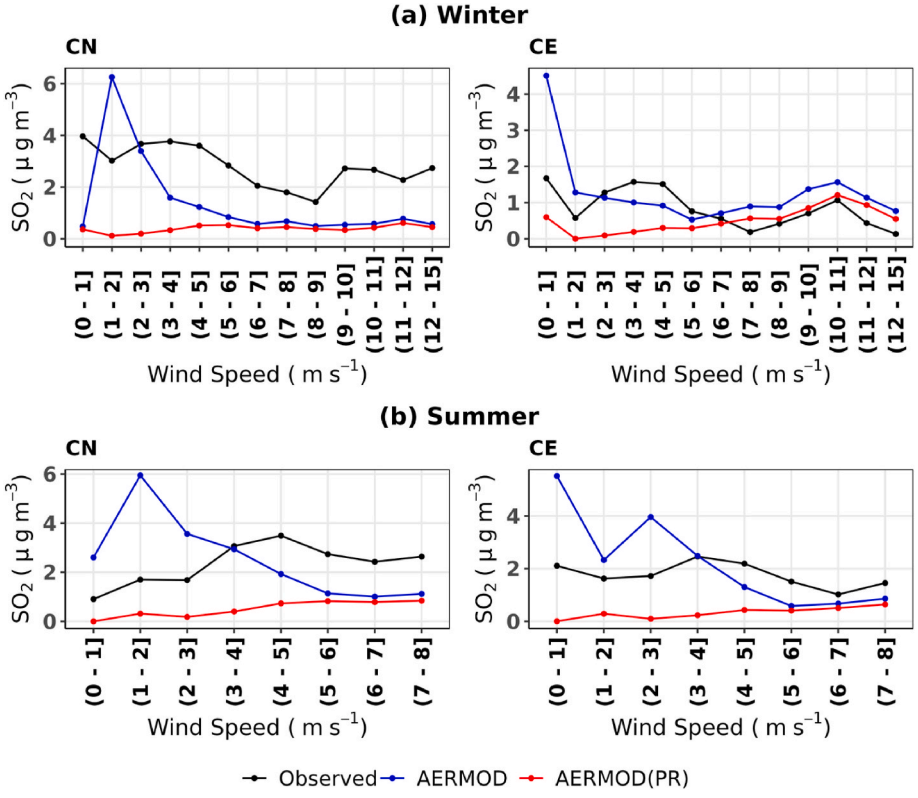

Fig. 8. Diurnal variation of SO_2 concentrations averaged over the two sites (CN and CE) with respect to each wind regime during winter (02/01/2012–02/29/2012) and summer seasons (07/18/2012–08/28/2012) of 2012.

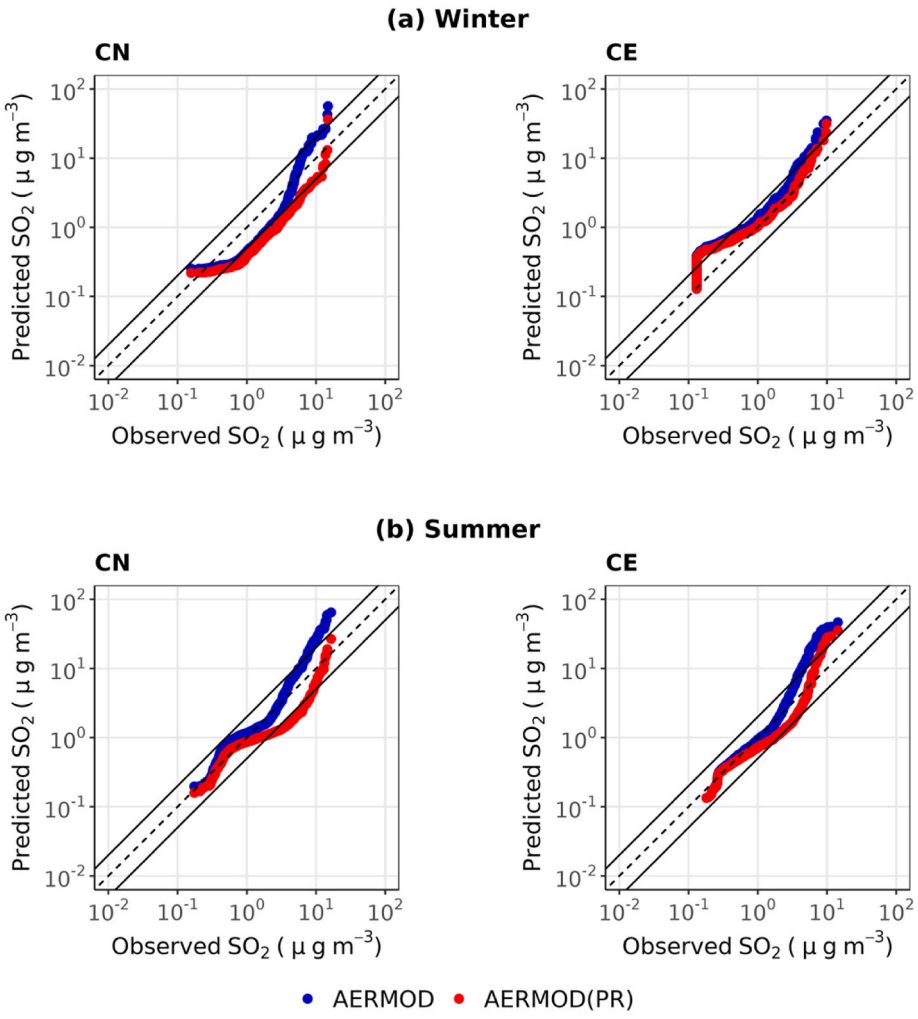

Fig. 9. Distribution of modeled SO_2 concentrations compared with that of observed concentrations measured at CN and CE during winter (02/01/2012 – 02/29/2012) and summer studies (07/18/2012 – 08/28/2012) of 2012.

model treats momentum-induced and buoyancy-induced plume rises as independent processes but incorporates interaction between these two processes. The variables used to compute plume rise are related to engine parameters that are routinely logged during aircraft operations. These parameters include fuel burn rate, thrust, aircraft velocity, bypass ratio, rated power, air-fuel ratio, and aircraft angle.

We find that the final plume rise associated with exhaust emissions from aircraft operating in LAX (an airport similar to large airports in the US, as well as in emerging global markets), is of the order of hundred meters at 1000 m from the source when an aircraft is taking off. It is much smaller when the aircraft is idling or taxiing. The proposed model for plume rise improves upon the constant value of initial spread of 16.1 m used to simulate aircraft emissions in AERMOD.

We evaluated the impact of incorporating plume rise in AERMOD by comparing AERMOD estimates, with and without plume rise, to measurements of SO_2 concentrations measured at two sites within LAX during a field study conducted in 2012. The measured SO_2 concentrations showed relatively small variation with wind speed when the flow was westerly, which is similar to the expected behavior seen by (Carslaw et al., 2006) in their analysis of data from Heathrow airport. The corresponding model estimates from AERMOD showed this type of behavior only when plume rise was incorporated into the model. We also show that the inclusion of plume rise in AERMOD improves the comparison between modeled and measured $\mathbf{SO_2}$ concentrations at LAX.

These results presented in this paper suggest the importance of incorporating plume rise in AERMOD in estimating the impact of aircraft emissions on air quality in areas downwind of airports. More detailed evaluation with measurements of plume rise at a large airport is needed to further improve the formulation described in this paper. We plan to apply and evaluate the algorithm with additional airport air quality studies in an extension of this study in multiple airports, both within and outside the U.S.

CRediT authorship contribution statement

Gavendra Pandey: Conceptualization, Methodology, Software, Data curation, Investigation, Formal analysis, Visualization, Writing – original draft. **Akula Venkatram:** Conceptualization, Methodology, Validation, Writing – review & editing. **Saravanan Arunachalam:** Conceptualization, Methodology, Project administration, Supervision, Funding acquisition, Writing – review & editing.

Declaration of competing interest

The authors declare that they have no known competing financial interests or personal relationships that could have appeared to influence the work reported in this paper.

Data availability

Data will be made available on request.

Acknowledgments

This research work was funded by the U.S. Federal Aviation Administration Office of Environment and Energy through ASCENT, the FAA Center of Excellence for Alternative Jet Fuels and the Environment, project 19 through FAA Award Number 13-C-AJFE-UNC under the supervision of Jeetendra Upadhyay. ASCENT (Aviation Sustainability Center) (http://ascent.aero) is a U.S. DOT-sponsored Center of Excellence. We thank Jeetendra Upadhyay and Mohammed Majeed of the FAA, and Chris Owen and Matthew Porter of EPA's Office of Air Quality, Planning and Standards for their review and valuable feedback on the manuscript and for several helpful discussions. The authors wish to gratefully acknowledge the Los Angeles World Authority (LAWA) and the U.S. DOT Volpe Center for providing datasets from the LAX AQSAS Study and additional aircraft engine parameters, and to Chowdhury Moniruzzaman for some early work processing AEDT data for this study.

Appendix A. Supplementary data

Supplementary data to this article can be found online at https://doi.org/10.1016/j.atmosenv.2023.120106.

References

Aeronautics-Guide, 2022. Aircraft gas turbine engines types and construction [WWW Document]. URL. https://www.aircraftsystemstech.com/p/gas-turbine-engines-types-and.html?m=1, 12.21.22.

Arunachalam, S., Valencia, A., Woody, M.C., Snyder, M.G., Huang, J., Weil, J., Soucacos, P., Webb, S., 2017. Airport cooperative research program, transportation research board, national academies of sciences, engineering, and medicine. In: Dispersion Modeling Guidance for Airports Addressing Local Air Quality Health Concerns. Transportation Research Board, Washington, D.C. https://doi.org/10.17226/24881.

Barrett, S.R.H., Britter, R.E., Waitz, I.A., 2013. Impact of aircraft plume dynamics on airport local air quality. Atmos. Environ. 74, 247–258. https://doi.org/10.1016/j.atmosenv.2013.03.061.

Briggs, G.A., 1965. A plume rise model compared with observations. J. Air Pollut. Control Assoc. 15, 433–438. https://doi.org/10.1080/00022470.1965.10468404.

Carruthers, D., McHugh, C., Jackson, M., Johnson, K., 2011. Developments in ADMS-Airport to take account of near field dispersion and applications to Heathrow Airport. Int. J. E Polit. 44, 332. https://doi.org/10.1504/IJEP.2011.038434.

Carslaw, D., Beevers, S., Ropkins, K., Bell, M., 2006. Detecting and quantifying aircraft and other on-airport contributions to ambient nitrogen oxides in the vicinity of a large international airport. Atmos. Environ. 40, 5424–5434. https://doi.org/10.1016/j.atmosenv.2006.04.062.

Carslaw, D.C., Ropkins, K., Laxen, D., Moorcroft, S., Marner, B., Williams, M.L., 2008. Near-field commercial aircraft contribution to nitrogen oxides by engine, aircraft type, and airline by individual plume sampling. Environ. Sci. Technol. 42, 1871–1876. https://doi.org/10.1021/es071926a.

CERC, 2020. ADMS - Airport (Version 5.0) Technical Specification. Cambridge Environmental Research Consultants.

Cimorelli, A.J., Perry, S.G., Venkatram, A., Weil, J.C., Paine, R.J., Wilson, R.B., Lee, R.F., Peters, W.D., Brode, R.W., 2005. AERMOD: a dispersion model for industrial source applications. Part I: general model formulation and boundary layer characterization. J. Appl. Meteorol. 44, 682–693. https://doi.org/10.1175/JAM2227.1.

FAA, 2014. Aviation environmental Design Tool (AEDT) [WWW Document]. https://aedt.faa.gov/. https://aedt.faa.gov/, 7.30.22.

Herbert, A., 2022. Turbojet vs. Turbofan: safety, efficiency, and performance – airplane academy [WWW Document]. URL. https://airplaneacademy.com/turbojet-vs-turbofan-safety-efficiency-and-performance/, 12.20.22.

Janicke, U., Janicke, L., 2007. Lasport - a model system for airport-related source systems based on a Lagrangian particle model. In: Presented at the 11th International Conference on Harmonization within Atmospheric Dispersion Modeling for Regulatory Purposes. HARMO, Cambridge, England, pp. 352–356, 2007.

Pandey, G., Venkatram, A., Arunachalam, S., 2022. Evaluating AERMOD with measurements from a major U.S. airport located on a shoreline. Atmos. Environ., 119506 https://doi.org/10.1016/j.atmosenv.2022.119506.

Perry, S.G., Cimorelli, A.J., Paine, R.J., Brode, R.W., Weil, J.C., Venkatram, A., Wilson, R. B., Lee, R.F., Peters, W.D., 2005. AERMOD: a Dispersion model for industrial source applications. Part II: model performance against 17 field study databases. J. Appl. Meteorol. 44, 694–708. https://doi.org/10.1175/JAM2228.1.

Tetra Tech, Inc, 2013. LAX air quality and source apportionment study. Los Angeles World airports. Available at: http://www.lawa.org/airQualityStudy.aspx?id=7716.

Venkatram, A., Schulte, N., 2018. Urban Transportation and Air Pollution. Elsevier. https://doi.org/10.1016/C2016-0-01641-8.

Wayson, R.L., Fleming, G.G., Kim, B., Eberhard, W.L., Brewer, W.A., 2004. Final Report: the Use of LIDAR to Characterize Aircraft Initial Plume Characteristics (No. FAA-AEE-04-01. FAA. DTS-34-FA34T-LR3.

Wayson, R.L., Fleming, G.G., Noel, G., MacDonald, J., Eberhard, W.L., McCarty, B., Marchbanks, R., Sandberg, S., George, J., Iovinelli, R., 2008. Lidar Measurement of Exhaust Plume Characteristics from Commercial Jet Turbine Aircraft at The Denver International Airport (No. FAA-AEE-08-02). FAA.